Atmospheric Research 214 (2018) 150–162

Contents lists available at ScienceDirect

Atmospheric Research

journal homepage: www.elsevier.com/locate/atmosres

Evolution mechanism of synoptic-scale EAP teleconnection pattern and its relationship to summer precipitation in China

Lijuan Wang[a], Chao Wang[a,b,*], Dong Guo[a]

[a] Key Laboratory of Meteorological Disaster, Ministry of Education/Joint International Research Laboratory of Climate and Environment Change/Collaborative Innovation Center on Forecast and Evaluation of Meteorological Disasters/Science and Technology Innovation Team on Climate Simulation and Forecast, Nanjing University of Information Science & Technology, Nanjing 210044, China

[b] State Key Laboratory of Severe Weather, Chinese Academy of Meteorological Sciences, Beijing 100081, China

ARTICLE INFO

Keywords:
East Asia-Pacific pattern
Wave-activity flux
Extreme precipitation
Circulation pattern
Energy conversion

ABSTRACT

Using ERA-Interim reanalysis daily data and gridded precipitation dataset, the evolution mechanism of East Asia-Pacific (EAP) teleconnection pattern and its relationship to summer precipitation in China were investigated on synoptic timescales based on EOF analysis, composite analysis, and significance test. The results demonstrate that the evolution of synoptic-scale EAP pattern is identified as having a significant relationship with the energy propagation represented by the wave-activity flux (WAF). Such EAP-related WAFs show various features in different levels of the troposphere. In the lower troposphere, the WAF primarily points poleward from the Philippines, playing a vital role in triggering and maintaining the synoptic-scale EAP pattern. A middle tropospheric zonally distributed ridge/trough/ridge wave train provides a favorable westerly waveguide for the southeastward (eastward) energy propagation, converging with a relatively weak poleward WAF over mid-latitude (high-latitude) East Asia. Moreover, the upper-level EAP-related anomalies are partly influenced by two conspicuous eastward WAFs. One may favor the development of Okhotsk anticyclonic (positive) anomaly, and the other one related to the Silk-Road (SR) wave train along the Asian jet converges into the cyclonic (negative) anomaly to greatly strengthen it. Particularly, the highly efficient baroclinic energy conversion responsible for the self-maintenance of SR pattern is also crucial for reinforcing and maintaining this cyclonic anomaly for a prolonged period by extraction of available potential energy from basic flow. In addition, during EAP pattern lifetime, due to the strong moisture flux convergence and upper-level divergence, the long-lasting strong ascents of moist/warm air along a moist and thick layer, therefore induce the summer consecutive extreme precipitation in the middle and lower reaches of Yangtze River.

1. Introduction

East Asia-Pacific (EAP) teleconnection pattern also named as Pacific-Japan (PJ) teleconnection pattern is recognized as one of the dominant modes and the most influential patterns during boreal summer, with a north-south tripole structure between the equator and high-latitudes over East Asia, which reflects the concurrent behavior of the western Pacific subtropical high (WPSH), Mei-Yu front, and Okhotsk blocking high (Kawamura et al., 1996; Kosaka and Nakamura, 2006).

The evolution mechanism of this meridional pattern has attracted substantial scientific attentions on seasonal and interannual to interdecadal timescales (Nitta and Hu, 1996; Fujinami and Yasunari, 2009; Gong et al., 2017; Hu et al., 2018). Initially, Huang (1987) and Nitta (1987) revealed that EAP (PJ) pattern was largely triggered by the northward-propagating Rossby wave forced by the anomalous convective heating around the Philippine Sea. Recent studies emphasized the importance of upper-level quasi-stationary wave trains (Guan and Yamagata, 2003; Shi et al., 2009). Corresponding eastward propagating wave fluxes from Europe across Asia along the westerly jets play significant roles in the reinforcement and preservation of EAP pattern (Kosaka et al., 2012). For example, the eastward energy propagation along the Silk-Road (SR) wave train within the Asian jet areas contributes to the advance and intensification of the Mei-Yu front and the WPSH (Enomoto et al., 2003; Ding and Wang, 2005, 2007; Chen et al., 2008; Lu and Lin, 2009). With a more northern route, the energy propagation oriented eastward from the Ural blocking high along the subpolar jet can primarily strengthen the Okhotsk blocking high

* Corresponding author at: Key Laboratory of Meteorological Disaster, Ministry of Education, Nanjing University of Information Science & Technology, Nanjing, China.
E-mail address: onechao@nuist.edu.cn (C. Wang).

https://doi.org/10.1016/j.atmosres.2018.07.023
Received 17 April 2018; Received in revised form 18 July 2018; Accepted 23 July 2018
Available online 26 July 2018
0169-8095/

(Nakamura and Fukamachi, 2004; Wang and Zhang, 2015). Though many previous studies have documented these issues on monthly and interannual timescales, the role of energy propagation on the EAP evolution has received limited attentions on synoptic timescales (Shi et al., 2009; Li et al., 2017). Thus, a first goal of current study is to confirm the significance of different energy dispersions in the advance and maintenance of the synoptic-scale EAP pattern, clarifying the distinctions of EAP-related energy dispersions in different levels of the troposphere.

Additionally, various studies have revealed different climate impacts between the positive and negative EAP phases (Ambrizzi et al., 1995; Chen and Zhai, 2015). Accordingly, negative (positive) geopotential height anomalies over mid-latitude East Asia (the Sea of Okhotsk and the subtropical western Pacific) related to the positive EAP phase, result in severe floods in southern China and cool summers in Japan (Wang et al., 2000; Wakabayashi and Kawamura, 2004). In particular, the concurrent behavior and interaction between EAP pattern and other summer teleconnections may cause more extreme and consecutive rainfall in southern China (Wakabayashi and Kawamura, 2004; Wang and Wang, 2018). Thus, the EAP pattern has been widely considered as an effective predictor of East Asian summer monsoon climate anomalies on a seasonal timescale (Lau and Weng, 2002; Hsu and Lin, 2007). While negative EAP phase with less precipitation signals in China, is basically related to the Pacific typhoons or their remnants (Kawamura and Ogasawara, 2006; Choi et al., 2010). Few similarities between individual typhoon-induced precipitation cases lead to huge complexities and diversities of their mechanisms (Xu et al., 2014). Hence, negative EAP phase is not discussed in present article, EAP pattern refers in particular to positive EAP phase.

Although some attentions have been paid to the evolution and climate effects of EAP pattern on seasonal and interannual to inter-decadal timescales (Kosaka and Nakamura, 2006; Hsu and Lin, 2007), these issues have rarely been systematically discussed on synoptic timescales. Thus, the objective of this article is to illuminate the evolution mechanism of EAP pattern and its connection with summer precipitation in China on synoptic timescales. Quantifying the significance of the synoptic-scale EAP pattern in inducing summer precipitation is conducive to presenting a better understanding of the EAP-related anomalous circulation variations responsible for precipitation.

2. Data and methods

2.1. Data

Daily meteorological datasets utilized in present study are obtained from the European Centre for Medium-Range Weather Forecasts (ECMWF) Re-analysis (ERA-Interim) during 1979–2015, including air temperature (K), horizontal wind field ($m\,s^{-1}$), geopotential height (gpm), vertical p-velocity ($Pa\,s^{-1}$), and specific humidity ($g\,kg^{-1}$), with 17 regular pressure levels vertically and a spatial resolution of $2.5^\circ \times 2.5^\circ$ (Dee et al., 2011; https://www.ecmwf.int/).

Daily outgoing long-wave radiation (OLR) data during 1979–2015 are also used to characterize the intensity and position variations of EAP-related convective activity near the Philippines (Liebmann, 1996; http://www.noaa.gov/), which are derived from the National Oceanic and Atmospheric Administration (NOAA) satellites, with a spatial resolution of $2.5^\circ \times 2.5^\circ$.

Daily precipitation dataset (Chinese Ground Precipitation $0.5^\circ \times 0.5^\circ$ Gridded Dataset, V2.0) employed in present study is released by the National Meteorological Information Center (NMIC) and China Meteorological Administration (CMA). More details of this gridded precipitation dataset are described in NMIC (National Meteorological Information Center, 2010; http://cdc.cma.gov.cn/).

2.2. Methods

The principal statistical methods used in present study include the empirical orthogonal function (EOF) analysis, composite analysis, and the ordinary Student's t-test. EOF analysis, which decomposes a space-time field into spatial modes and associated time series, provides an effective way to identify and extract the synoptic-scale EAP mode during East Asian summer based on daily geopotential height field (North et al., 1982; Loboda et al., 2005; Hatzaki and Wu, 2015). Composite analysis is a widely employed and simple yet effective tool in identifying typical synoptic to sub-monthly scale circulation patterns and their precursors related to extreme precipitation cases, and the purpose of ordinary Student's t-test is to achieve more rigorous statistical significance thresholds (Grotjahn and Faure, 2008; Chen and Zhai, 2016).

As suggested by Hart and Grumm (2001), for daily precipitation dataset, a 7-day binominal filter (3 days on either side of a particular day) is firstly used to highlight the daily variability. Accordingly, daily climatological mean value and standard deviation (σ) are calculated by use of the above smoothed daily precipitation data during 1979–2015. This unequal-weighed binominal filter is designed to dampen chaotic very-high-frequency signals and retain strong precipitation signals substantially (Chen and Zhai, 2015; Wang and Wang, 2018). For the other variables associated with the synoptic-scale EAP pattern, such as geopotential height and horizontal wind fields, a 21-day binominal filter seems more suitable (Grumm and Hart, 2001). The standard deviation and climatological mean value calculated by these smoothed data seem to be more stable compared with only using the unsmoothed single-day values. Hence, we can calculate the normalized anomaly of a variable on a particular day as follows: aiming to retain the synoptic signal mostly, corresponding climatological daily mean is firstly subtracted; then the value is divided by the corresponding climatological daily standard deviation.

Diabatic heating anomalies can cause the variations of vorticity in both the lower and upper troposphere, thereby affecting the circulation pattern (Hsu and Weng, 2001). To investigate the impact of atmospheric diabatic heating on EAP-related circulation variations, the apparent heat source (Q) is therefore calculated according to the widely-used scheme deduced by Yanai et al. (1973) based on ERA-Interim daily observational datasets; that is,

$$Q = c_p\left[\frac{\partial T}{\partial t} + \vec{V}\cdot\nabla_h T + \left(\frac{p}{p_0}\right)^{R/c_p}\omega\frac{\partial\theta}{\partial p}\right] \tag{1}$$

In Eq. (1), c_p, R, and T denote the specific heat of dry air at constant pressure, the gas constant for dry air, and the air temperature respectively, $p_0 = 1000$ hPa (Yanai et al., 1973). $\vec{V}$ is the horizontal vector winds, p the pressure, ω the vertical p-velocity, θ the potential temperature, and ∇ is the isobaric gradient operator.

The wave-activity flux (WAF) is calculated to describe the energy propagation characteristics of quasi-stationary waves and transient fluctuations in this study (Takaya and Nakamura, 1997, 2001). Concretely, the WAF is phase-independent under the assumption of the Wentzel–Kramers–Brillouin (WKB) approximation, which tends to be consistent with the local group velocity direction of quasi-stationary Rossby wave train. The two-dimensional formula can be expressed as:

$$W = \frac{p}{2000\,|\vec{U}|}\begin{Bmatrix} U(\psi'^{2}_{x} - \psi'\psi'_{xx}) + V(\psi'_{x}\psi'_{y} - \psi'\psi'_{xy}) \\ U(\psi'_{x}\psi'_{y} - \psi'\psi'_{xy}) + V(\psi'^{2}_{y} - \psi'\psi'_{yy}) \end{Bmatrix} \tag{2}$$

where ψ' denotes the stream function for quasi-geostrophic flow. $\vec{U} = (U, V)$ is the horizontal zonally varying basic flow, U and V represent the zonal and meridional wind components respectively, p signifies the pressure (hPa). The climatological daily mean flow during summer (June–August) from 1979 to 2015 is used as the basic flow, including zonal and meridional wind fields with zonal nonuniformity.

Thus, this formula is suitable for the complex mid-high latitude circulation patterns (Kosaka and Nakamura, 2006; Li et al., 2017).

Besides, EAP pattern usually coexists with two major teleconnection patterns in the Northern Hemisphere summertime: Silk-Road (SR) and Eurasian (EU) patterns (Wakabayashi and Kawamura, 2004; Wang and Wang, 2018). To clarify the influence of their coexistence or interaction on the development and maintenance of synoptic-scale EAP pattern, this study also defines the daily indices of SR and EU patterns (referred to as SRI and EUI, respectively):

$$\mathrm{SRI} = [Z^*_{200}(65^{\circ}\mathrm{E}, 40^{\circ}\mathrm{N}) - Z^*_{200}(100^{\circ}\mathrm{E}, 40^{\circ}\mathrm{N}) + Z^*_{200}(130^{\circ}\mathrm{E}, 40^{\circ}\mathrm{N})]/3 \quad (3)$$

$$\mathrm{EUI} = [Z^*_{500}(45^{\circ}\mathrm{E}, 60^{\circ}\mathrm{N}) - Z^*_{500}(100^{\circ}\mathrm{E}, 65^{\circ}\mathrm{N}) + Z^*_{500}(145^{\circ}\mathrm{E}, 60^{\circ}\mathrm{N})]/3 \quad (4)$$

where the Z_{200}^* and Z_{500}^* denote the 200 hPa and 500 hPa normalized geopotential height anomalies, respectively (Wakabayashi and Kawamura, 2004).

Kosaka and Nakamura (2006) have indicated that the barotropic (*CK*) and baroclinic (*CP*) energy conversions from the climatological-mean flow can replenish the total energy required by EAP pattern. Thus, it is necessary to examine the dynamics of synoptic-scale EAP pattern and the importance of energy conversions in maintaining and reinforcing the EAP-related anomalous circulation pattern. The *CK* and *CP* are formulated as:

$$CK = \frac{v'^2 - u'^2}{2}(\partial\bar{u}/\partial x - \partial\bar{v}/\partial y) - u'v'(\partial\bar{u}/\partial y + \partial\bar{v}/\partial x) \quad (5)$$

and

$$CP = -(f/S)(v'T'\partial\bar{u}/\partial p - u'T'\partial\bar{v}/\partial p) \quad (6)$$

respectively. In Eqs. (5) and (6), u and v represent the zonal and meridional wind components; p is pressure, f the Coriolis parameter, T temperature, and S denotes the stability parameter $S = R\bar{T}/C_p p - \partial\bar{T}/\partial p$ with C_p the specific heat of the air at the constant pressure and R the gas constant of dry air. Positive *CK* and *CP* signify that the anomalies extract kinetic energy (*KE*) and available potential energy (*APE*), respectively, from the basic state (Sato and Takahashi, 2006).

In order to further investigate the net contributions from energy conversions in the key region, the efficiencies of energy conversions are evaluated as the time scales given by (Simmons et al., 1983; Kosaka and Nakamura, 2006)

$$\tau_{CK} = [KE]/[CK] \quad (7)$$

$$\tau_{CP} = [APE]/[CP] \quad (8)$$

and

$$\tau_{CK+CP} = [KE + APE]/[CK + CP] \quad (9)$$

Here, [ ] denotes the vertical integration. The positive and negative values of time scales represent the net energy gain and loss, respectively. Any process whose time scales for the energy gain is < 3 days may be considered as being effective for strengthening and maintaining the synoptic anomalies associated with synoptic-scale EAP pattern (Simmons et al., 1983; Kosaka et al., 2009).

3. Definition of synoptic-scale EAP pattern

The synoptic-scale EAP teleconnection pattern shows a meridional tripole structure, which is consistent with the interannual and interdecadal EAP pattern (Kosaka and Nakamura, 2006). The similar north-south tripole structure ('+ − +') is clearly identified by the dominant EOF mode of daily 500 hPa normalized height anomalies over East Asia (110–150°E, 0–75°N) in summer (June–August) during 1979–2015 with 14.96% explained variance (Fig. 1).

Then, a daily EAP index (EAPI) is defined. Firstly, three basic points

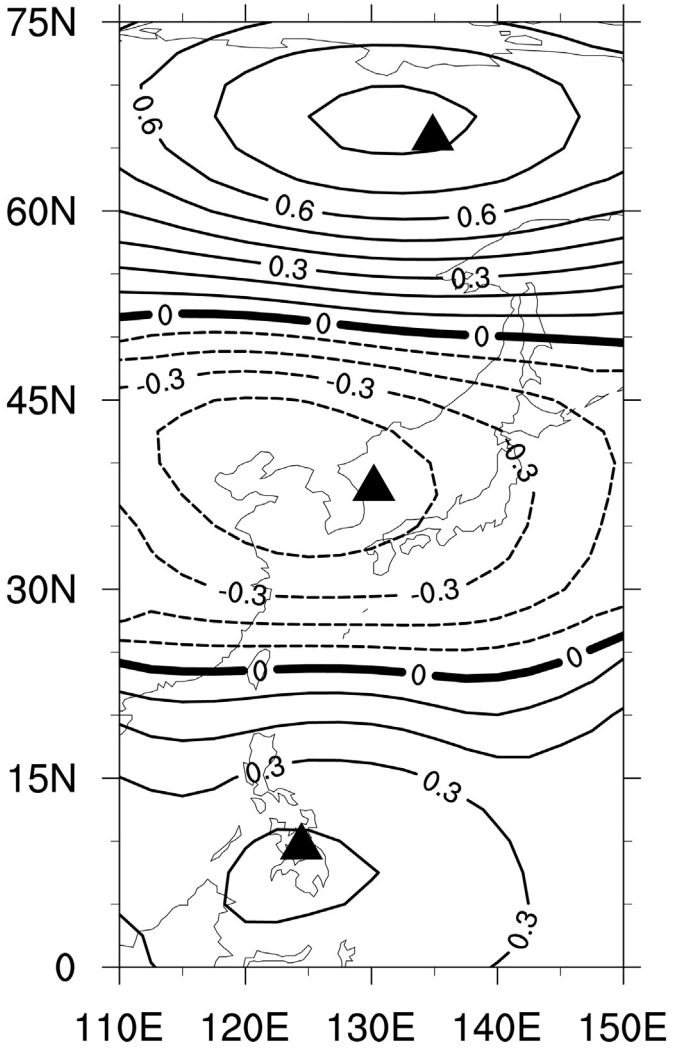

Fig. 1. The first EOF mode of daily 500 hPa normalized height anomalies in East Asia (110–150°E, 0–75°N) during summertime (June–August) from 1979 to 2015. Dashed and solid contours signify the negative and positive values, respectively (with interval of 0.1). The triangles represent the three basic points in Eq. (10).

selected to represent three anomaly centers of synoptic-scale EAP pattern are (125°E, 10°N) over the tropical western Pacific, (130°E, 37.5°N) over mid-latitude East Asia, and (135°E, 65°N) over the Sea of Okhotsk, based on the first mode of EOF analysis (Fig. 1). Secondly, EAPI is calculated by use of daily normalized 500 hPa geopotential height anomalies at these three basic points (Eq. (10)).

$$EAPI = (H_{WP} - H_{EA} + H_{SO})/3 \quad (10)$$

where the H_{WP}, H_{EA}, H_{SO} represent the normalized geopotential height anomalies at 500 hPa of the three basic points in Fig. 1, respectively.

Synoptic-scale EAP (referred to as positive phase) events are identified, after the EAPI being defined. A typical synoptic-scale EAP event must satisfy the following three criteria simultaneously. (1) EAPI is > 1.0 standard deviation (σ) for at least three consecutive days. (2) Height anomalies at 500 hPa show the tripole structure as '+ − +' corresponding to the three basic points. (3) Time interval between two EAP events must be > 15 days. In total, 19 EAP events are identified (Table 1), according to the criteria.

To ensure an adequate sample size, the relaxed thresholds of both the duration and intensity are necessary for identifying the anomalous circulation regimes (Archambault et al., 2010). Both the three consecutive days and one standard deviation were broadly accepted as the

Table 1
The year, start date, end date, duration (days), averaged EAPI, and averaged H_{WP}, H_{EA}, H_{SO} of the 19 EAP events.

Year	Start date	End date	Duration	EAPI	H_{WP}	H_{EA}	H_{SO}
1983	6 July	8 July	3	1.54	1.77	−1.90	0.96
1986	5 July	8 July	4	1.51	1.04	−1.66	1.84
1988	15 June	17 June	3	1.69	1.35	−1.69	2.05
1989	16 June	18 June	3	1.70	1.79	−1.90	1.43
1991	2 July	11 July	10	1.80	1.90	−1.47	2.03
1992	14 June	18 June	5	1.45	1.39	−1.50	1.45
1993	21 July	25 July	5	2.16	1.47	−2.44	2.56
1995	19 June	3 July	15	2.19	1.63	−2.62	2.31
1996	17 June	19 June	3	1.79	2.34	−1.97	1.07
1998	9 June	20 June	12	2.34	1.86	−2.00	3.17
1998	19 July	24 July	6	2.01	1.29	−2.18	2.55
1999	15 July	19 July	5	1.78	1.05	−1.71	2.58
2000	7 June	10 June	4	1.83	1.63	−2.38	1.48
2002	12 June	18 June	7	1.89	1.93	−2.03	1.72
2006	8 June	11 June	4	1.73	1.56	−1.79	1.84
2008	21 June	29 June	9	1.98	2.33	−1.45	2.18
2009	11 June	16 June	6	2.06	1.82	−2.77	1.59
2012	8 June	20 June	13	1.92	1.78	−1.91	2.07
2015	1 July	3 July	3	1.67	2.06	−1.96	0.98

typical duration and intensity in various studies (Chen and Zhai, 2015; Lü et al., 2017). On an average, there is less than one EAP event per summer can be selected from the EAPI during 1979–2015 (approximately 37 summers). It is possible that though the EAP pattern also emerges in some summers, but its intensity and duration fail to satisfy the criteria of 'a typical EAP event', a daily EAPI value of 1.0σ or greater remaining for less than three consecutive days. Further considering the complexity of East Asian summer circulations (Ding and Chan, 2005; Jin et al., 2013; Chen et al., 2017), these identified 19 EAP events can be basically regarded as the typical cases to investigate the evolution mechanism and the relationship with summer rainfall in China.

The following composite analyses are generally based on these identified 19 typical EAP cases. For convenience, day 0 represents the start date (Table 1) of EAP events, day (*n*) denotes the day prior to (negative) and after (positive) the start date of EAP events in this study.

4. Evolution features and mechanism of synoptic-scale EAP pattern

Though EAP pattern was initially recognized as being confined in the lower troposphere (Huang, 1987; Nitta, 1987), subsequent studies emphasized its vertical structure (Kosaka and Nakamura, 2006). Therefore, this section mainly illuminates the evolution characteristics and mechanism of synoptic-scale EAP pattern in the lower, middle, and upper troposphere respectively, discussing the importance of the wave-activity flux (WAF) which reflects the energy propagation of Rossby wave-like perturbation (Hsu and Lin, 2007; Fujinami and Yasunari, 2009).

4.1. Evolution of synoptic-scale EAP pattern in the lower troposphere

Prior to the onset of typical EAP events, a positive height anomaly of 1.5σ above normal tends to be anchored to the west of the Ural Mountains for a few days at 850 hPa (Fig. 2). During this period, no obvious eastward-pointing WAFs can be identified from this positive anomaly to East Asia, which indicates a trivial contribution of energy dispersion from the Ural Mountains to East Asia on the EAP evolution at 850 hPa. It suggests that the dynamical connection between Europe and East Asia is less pronounced in the lower troposphere (Shi et al., 2009).

At low-latitudes, during the developing phase of EAP pattern, the suppressed convective activity (indicated by the positive OLR anomalies in Fig. 2) in the vicinity of the Philippines begins to shift westward and strengthen saliently from day −6 onward, followed by a positive height anomaly of 1.0σ above normal, inducing the low-level anomalous diabatic cooling (Fig. 2a). These convective cooling anomalies therefore trigger the poleward energy propagation from the Philippine Sea, which can be confirmed by the northward-pointing WAFs. It was widely accepted that the poleward energy dispersion was mainly attributed to the anomalous convections around the Philippines (Huang and Sun, 1994; Li et al., 2017). By day −4, the poleward WAF is discernible and reaches 35°N, which can stimulate the following formation of the mid-latitude negative height anomalies over −1.0 standard deviation. Subsequently, both the low-latitude positive height anomaly and convective cooling anomalies strengthen markedly and shift westward concurrently (Fig. 2c). After day −2, the enhanced convective cooling anomalies further reinforce the poleward WAFs (Huang and Sun, 1994). These poleward WAFs, which can reach 60°N, provide favorable wave energy for the early development of positive height anomaly over the Sea of Okhotsk (Nitta and Hu, 1996).

Then the well-organized meridional tripole structure of synoptic-scale EAP pattern completely forms at 850 hPa on day 0. During its lifetime, the long-lasting poleward energy dispersion maintains this meridional tripole structure for several days (Fig. 2). Similar findings have been documented by Kosaka and Nakamura (2006). They pointed out that the interannual variability of PJ teleconnection pattern was determined by the barotropic Rossby wave propagation arising from the tropical diabatic heating anomalies. At the decaying stage (approximately after day 4), the dissipation of poleward energy propagation resulting from the decay of anomalous convective cooling around the Philippines rapidly weakens the anomalies related to synoptic-scale EAP pattern, thereby terminating EAP events (figure not shown).

It is interesting to note that the poleward energy dispersion forced by the anomalous convective cooling around the Philippines triggers the three EAP-related synoptic anomaly centers in sequence from low- to mid-high latitudes over East Asia and maintains the tripole structure for > 3 days (Huang and Sun, 1994; Nitta and Hu, 1996).

4.2. EAP-related energy propagation in the middle troposphere

The middle tropospheric (500 hPa) large-scale circulation is significantly characterized by the double-blocking highs centered over the Ural Mountains and the Sea of Okhotsk respectively, with a long-lived and broad trough between them (Fig. 3). From day −6 onward, the zonally distributed ridge/trough/ridge wave train, resembling the West Europe-Japan (EJ) wave train (Wakabayashi and Kawamura, 2004) or Eurasian (EU) teleconnection pattern (Wang and Zhang, 2015), provides a favorable zonally-elongated westerly waveguide for the eastward propagating WAFs from the Ural blocking high areas (Ambrizzi et al., 1995; Takaya and Nakamura, 2001). On day −2, the composite 500 hPa normalized height anomalies shows that EU-like pattern exhibits three significant anomaly centers with reverse signs (Fig. 3c), which can be confirmed by the composite EUI of > 0.75σ remaining from day −2 to day 4 (Fig. 7a). Consequently, the eastward energy propagation along this westerly waveguide strengthens saliently and reaches the high-latitude East Asia, further reinforcing the Okhotsk high with positive height anomalies of 1.0σ above normal. In addition, the southeastward WAFs can also be detected from the Ural Mountains to mid-latitude East Asia, slightly deepening the mid-latitude trough (Li et al., 2017).

At low-latitudes, the period from day −6 to day −2 portrays the westward extension of the WPSH (588 dagpm-contours), followed by a westward-progressive positive height anomaly of 1.0σ above normal, which results in a considerable growth of poleward WAFs from tropics. Subsequently, the convergence (Fig. 3c) between these poleward WAFs and the aforementioned southeastward WAFs over mid-latitude East Asia sharply deepens the trough with negative height anomalies of 1.0σ below normal (Chen and Zhai, 2015). Thereafter, the further enhancement and westward extension of the WPSH strengthen the EAP-related poleward energy dispersion markedly (Nitta, 1987; Huang and

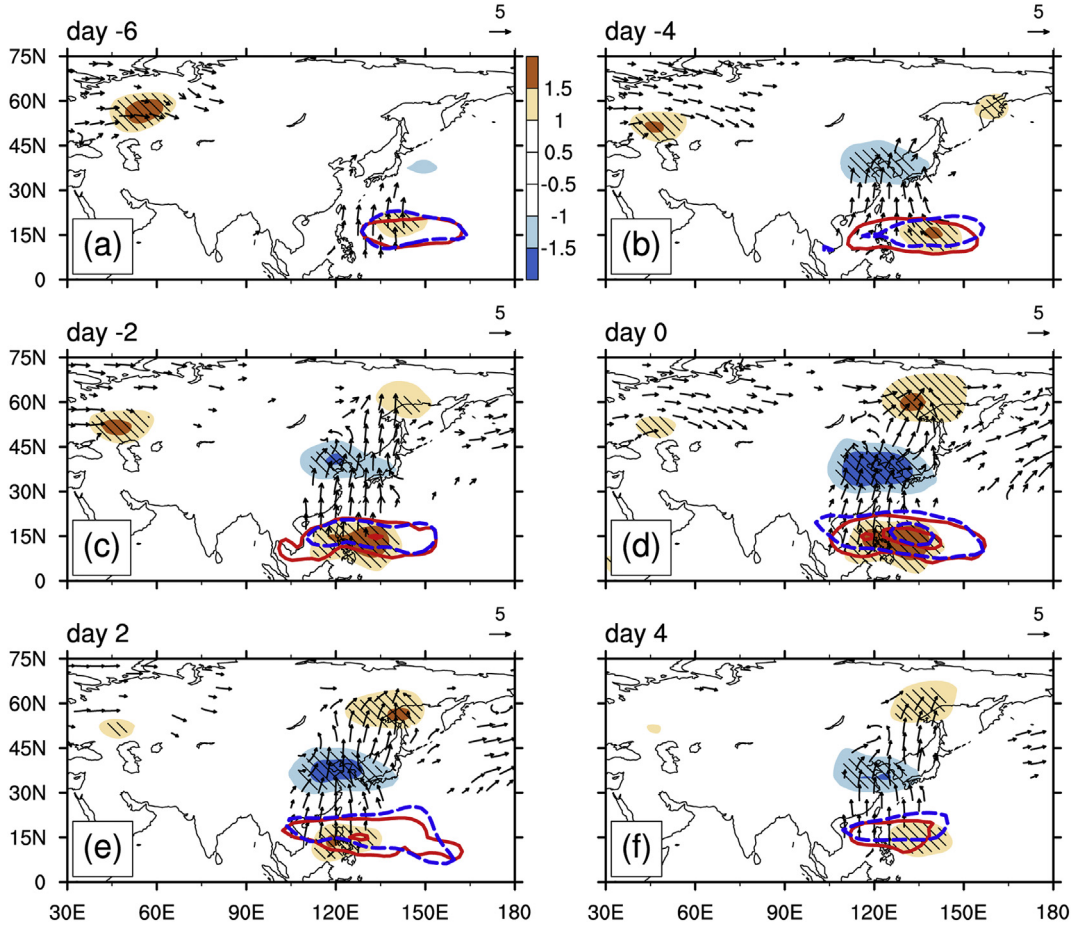

Fig. 2. Composite 850 hPa normalized height anomalies (shading), anomalies of outgoing long-wave radiation (OLR, red contours are +25, +50 W m^{-2}), wave-activity flux (vector; units: m^2 s^{-2}), and diabatic heating anomalies (blue contours are −1.0, −1.5 K day^{-1}). Statistically significant height anomalies (5% level) are highlighted by diagonal lines. Wave fluxes < 2.0 m^2 s^{-2} are not drawn. The numbers at the bottom-left corner above each panel represent the days lagging (positive) and leading (negative) the onset of EAP events. (For interpretation of the references to colour in this figure legend, the reader is referred to the web version of this article.)

Sun, 1994; Ding and Chan, 2005; Jiang et al., 2005). The persistent convergence between the poleward WAFs and southeastward WAFs at mid-latitudes further deepens the trough with negative height anomalies of 1.5σ below normal. Meanwhile, the poleward WAFs from the mid-latitudes to the Sea of Okhotsk also experiences an increase, with a similar convergence between the poleward WAF and eastward WAF at high-latitudes. This convergence further enhances the Okhotsk blocking high, with intensity of positive anomalies exceeding 1.5σ on day 0 (Li et al., 2017).

After day 0, the synoptic-scale EAP pattern becomes well-established at 500 hPa and remains for at least 3 days (Fig. 3d). During its lifetime, the long-lasting ridge/trough/ridge circulation pattern provides a persistent westerly waveguide for the eastward and southeastward energy propagations, maintaining and reinforcing the mid-latitude trough and the Okhotsk blocking high. At decaying stage, as the WPSH retrogrades eastward to its climatological mean position after day 4, the low-latitude positive height anomaly vanishes firstly arising from the dissipation of poleward energy dispersion (Fig. 3f). As a result of the decay of the Ural blocking high, the westerly waveguide weakens immediately, and both the eastward and southeastward energy propagations therefore fail to be sustained, terminating EAP events (figure not shown).

Different from the lower troposphere, the WAFs show a distinctive and unique feature in the middle troposphere, this is, the significant convergences of the meridional WAFs and zonal WAFs, which are responsible for the steady progression and preservation of synoptic-scale EAP pattern. Furthermore, this may be the primary cause why the three anomaly centers of synoptic-scale EAP pattern appear simultaneously in the middle troposphere (Kosaka and Nakamura, 2006).

4.3. Upper-level evolution and the association with energy propagation

The temporal variation features of synoptic-scale EAP pattern in the upper troposphere (200 hPa) are illustrated in Figs. 4 and 5. In the developing phase (from day −6 to day 0), the typical EAP events start with a positive height anomaly of 1.0σ above normal located to the west of the Ural Mountains, which shifts westward and weakens gradually. Noticeably, the more pronounced eastward WAFs, persistently emanating from this positive height anomaly, stimulate the early development of the high-latitude anticyclonic anomaly with positive height anomalies of 0.5σ above normal on day −2 (Chen et al., 2008). Meanwhile, with a more southern route, the mid-latitude WAF emanating from the Iranian plateau is oriented eastward along the upper-level Asian jet (Fig. 4c), which tends to shift southeastward along the northerlies to the eastern flank of the South Asia High (SAH, 12520 gpm-contours in Fig. 5). Then it converges into the mid-latitude cyclonic anomaly to greatly enhance it, with negative height anomalies of 1.5σ below normal. Particularly, the similar upper-level wave energy dispersions have also been highlighted in previous studies (Kosaka and Nakamura, 2006; Hsu and Lin, 2007; Fujinami and Yasunari, 2009).

After day −2, as the SAH stretches eastward to east of 120°E, the westerly jet accelerates manifestly and displaces equatorward to 30°N,

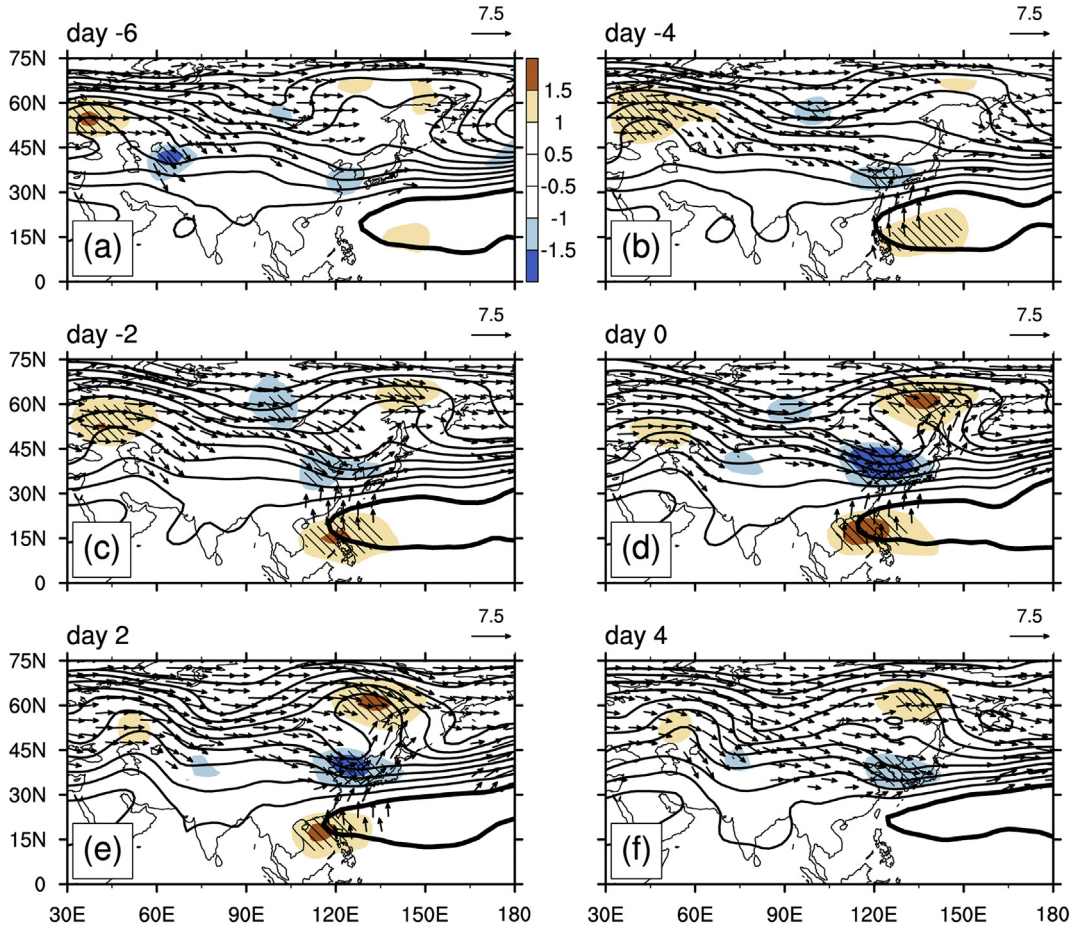

Fig. 3. Composite 500 hPa geopotential height field (contours are from 552 to 588 dagpm with interval of 4 dagpm), normalized height anomalies (shading), and wave-activity flux (vector; units: $m^2 s^{-2}$). The thick contours (588 dagpm-contours) represent the boundaries of the WPSH. Statistically significant height anomalies (5% level) are highlighted by diagonal lines. Wave fluxes $< 2.5\ m^2 s^{-2}$ are not drawn.

enhancing the northerlies prevailing to the northeast of the SAH (Fig. 5c). The mid-latitude cyclonic anomaly embedded in these northerlies intensifies substantially, with a zonally elongated structure, resulting in a sharper meridional height gradient with negative height anomalies of 2.0σ below normal. At day 0, both the mid- and high-latitude anomalies related to synoptic-scale EAP pattern are clearly identified at 200 hPa, with the absence of low-latitude anomaly center (Kosaka and Nakamura, 2006). It may imply that the synoptic-scale EAP pattern shows an equivalent barotropic structure in the mid-high latitudes and the baroclinic structure at low-latitudes in vertical direction (Nitta, 1987).

In addition, another significant wave train dominates in the upper troposphere within the Asian jet areas from day −2 onward, which is called the Silk-Road (SR) pattern (Lu et al., 2002; Hong and Lu, 2016) or West Asia-Japan pattern (Kosaka et al., 2012), with the alternating quasi-stationary cyclonic and anticyclonic anomaly centers (anomalous cyclone/anticyclone/cyclone wave train in Fig. 5) aligned in a near-zonal direction. Also, composite indices clearly show that the SRI value of −1.0σ or less remains from day −1 to day 5. It reflects the long-lasting simultaneous existence and concurrent behavior of the EAP pattern and SR pattern in the upper troposphere (Wakabayashi and Kawamura, 2004; Kosaka et al., 2009). Accordingly, the development and maintenance of mid-latitude cyclonic anomaly is partly under the influence of the SR-related eastward energy propagation for a prolonged period (from day −2 to day 4).

Of particular note are the marked distinctions among different heights. (1) Convection-induced poleward energy propagation is clearly identified in the lower troposphere, which decreases with height, instead of the southeastward dispersion from the mid-latitudes to tropics at 200 hPa. (2) Due to the existence of the westerly waveguide and the westerly jet, the mid-latitude eastward WAFs are more pronounced in the mid-to-upper troposphere than that in the lower troposphere (Ding and Wang, 2005). (3) The distinct convergences between the zonal and meridional WAFs mainly occur in the middle troposphere (Shi et al., 2009).

4.4. Energetics of the EAP pattern

As previously reported, the SR teleconnection pattern had a characteristic and dynamic of a quasi-stationary Rossby wave train, which could be commonly maintained by extracting the kinetic energy from the basic flow through the barotropic and baroclinic energy conversions (Sato and Takahashi, 2006; Kosaka et al., 2009). The concurrent behavior of the SR and EAP patterns attracts attentions for the role of energy conversions in maintaining and reinforcing themselves.

Fig. 6 presents the spatial distributions of vertically-integrated *CK* and *CP* in the developing and peak phases of EAP events. It demonstrates that both the *CK* and *CP* are mainly concentrated around the Asian jet areas, with the strongest *KE* extraction into the SR pattern on the northern flank of the western core of the Asian jet (45–60°E), and the large positive values of *CP* are near the Caspian Sea (day −6). From day −4, a wave-like distribution of baroclinic energy conversion is quite similar to the SR pattern. This is consistent with the conclusions drawn by Kosaka et al. (2009), which confirms the dominance of barotropic and baroclinic energy conversions in the self-maintenance and geographical fixing of the SR pattern (Wakabayashi and Kawamura,

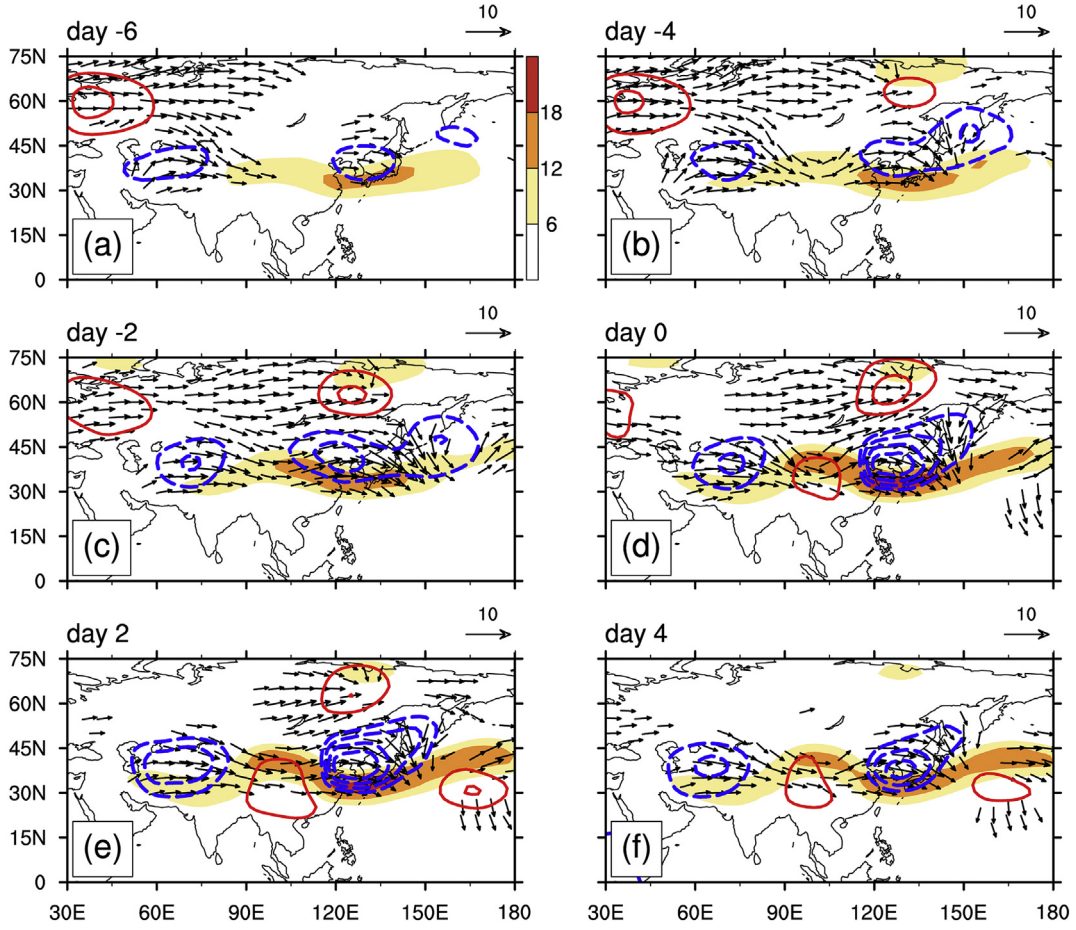

Fig. 4. Composite 200 hPa normalized height anomalies (contours denote ± 0.5, ± 1.0, ± 1.5, ± 2.0 standard deviation, red for positive and blue for negative), zonal wind anomalies (shading; units: $m\,s^{-1}$), and wave-activity flux (vector; units: $m^2\,s^{-2}$). Wave fluxes < $4\,m^2\,s^{-2}$ are not drawn. (For interpretation of the references to colour in this figure legend, the reader is referred to the web version of this article.)

2004). On day −2, the large values of both *CK* and *CP* are also clearly identified around the cyclonic anomaly over mid-latitude East Asia. Thus, a key region (105–150°E, 32.5–45°N) is selected to diagnose the net contribution of energy conversions on the progression and preservation of this EAP-related cyclonic anomaly. The results manifest that both the barotropic and baroclinic energy conversions averaged in the selected key region convert to net positive energy conversions from day −2 (Fig. 7b). The extractions of *KE* and *APE* from the basic flow may be conducive to maintaining or reinforcing the cyclonic anomaly through the barotropic and baroclinic energy conversions (Sato and Takahashi, 2006).

The efficiencies of energy conversions are also summarized in Table 2. Within the key region, time scale of barotropic energy conversion (τ_{CK}) is approximately 23.5 days, which is much longer than the timescales of synoptic-scale EAP pattern. Consequently, the barotropic energy conversion, though stronger, is not efficiently enough (Simmons et al., 1983; Kosaka and Nakamura, 2006). But the time scale of baroclinic energy conversion (τ_{CP}) integrated vertically over the key region (105–150°E, 32.5–45°N) is 1.34 days and 0.24 days (5.76 h) during the developing and peak phases, respectively. It indicates the vital role of the baroclinic energy conversion in enhancing and maintaining the mid-latitude synoptic cyclonic anomalies. Therefore, the high efficiencies reveal that the mid-latitude cyclonic anomalies primarily gain *APE* from the basic flow to reinforce and maintain themselves through the baroclinic energy conversion, rather than the barotropic energy conversion (Sato and Takahashi, 2006; Kosaka et al., 2009).

5. Relationship with the summer precipitation in China

In the former analyses, the evolution characteritics and dynamics of synoptic-scale EAP pattern are investigated. This section will quantify the relationships between the synoptic EAP pattern and precipitation in China by use of composite analysis, followed by the temporal variation of daily normalized regionally averaged precipitation.

5.1. Distribution of precipitation associated with EAP pattern

To better capture the great impacts of synopotic-scale EAP pattern on summer rainfall, the days when EAPI remains above one standard deviation for at least three consecutive days are selected for composite analyses (Wang and Zhang, 2015), based on the identified 19 typical EAP cases listed in Table 1. The distribution of average precipitation during EAP events presented in Fig. 8 shows more rainfall signals in the Yangtze River's middle and lower reaches (27–32°N, 112.5–120°E). Daily normalized regionally averaged precipitation of 1.0σ or greater remains from day 0 to day 4 (Fig. 8b), which signifies the long-lasting precipitation of approximately 50 mm day^{-1} or greater (Fig. 9) at an individual station of precipitation center (Chen and Zhai, 2016). Although 50 mm day^{-1} is not particularly extreme during monsoonal season in the Yangtze River Valley, the accumulated precipitation amount of > 200 mm arising from its long duration (approximately 4–5 days) is probably to cause a severe, large-scale flood within just several days (Hsu and Lin, 2007).

In this study, the summer extreme precipitation cases are identified based on 1.0σ or greater of daily normalized regionally averaged

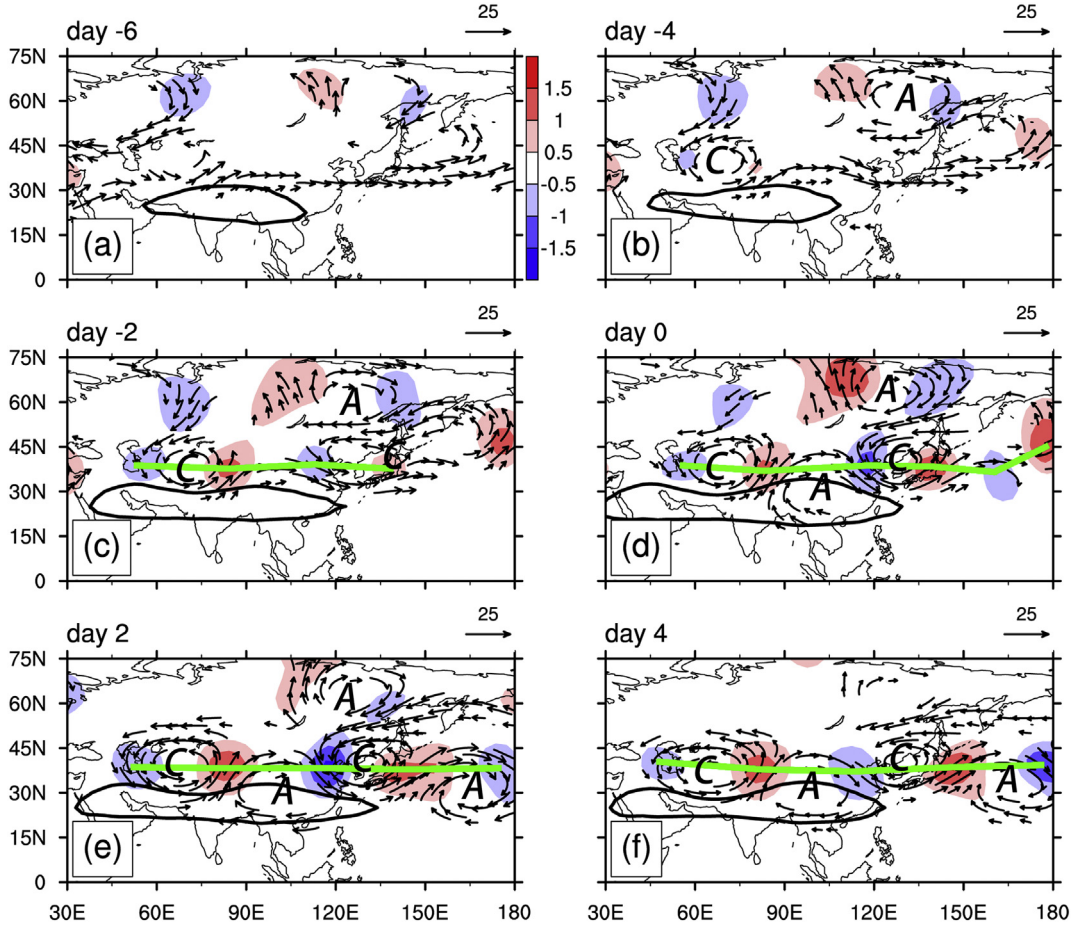

Fig. 5. Composite 200 hPa meridional wind anomalies (shading; units: m s^{-1}) and horizontal wind anomalies (vector; units: m s^{-1}). Statistically significant horizontal wind anomalies (at least 5% level) are plotted. Anomalous cyclone and anticyclone are represented by the letters 'C' and 'A', respectively. The black contours (12,520 gpm-contours) denote the boundaries of the SAH. The green lines represent the amplitude centers locations of the meridional wind anomalies at mid-latitudes. (For interpretation of the references to colour in this figure legend, the reader is referred to the web version of this article.)

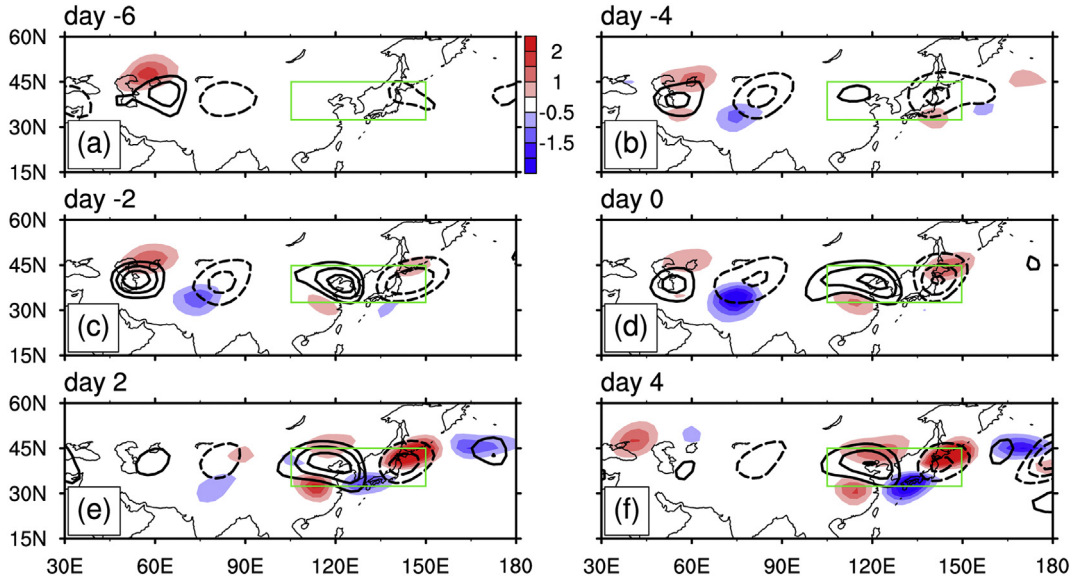

Fig. 6. Barotropic energy conversion *CK* (shading; units: W m^{-2}) and baroclinic energy conversion *CP* (contours are ± 0.5, ± 1.0, ± 1.5 W m^{-2}) integrated vertically from surface to 100 hPa level during the period from day −6 to day 4. The green rectangles denote the regions (105–150°E, 32.5–45°N) chosen for calculating the domain-averaged energy conversions in Fig. 7. (For interpretation of the references to colour in this figure legend, the reader is referred to the web version of this article.)

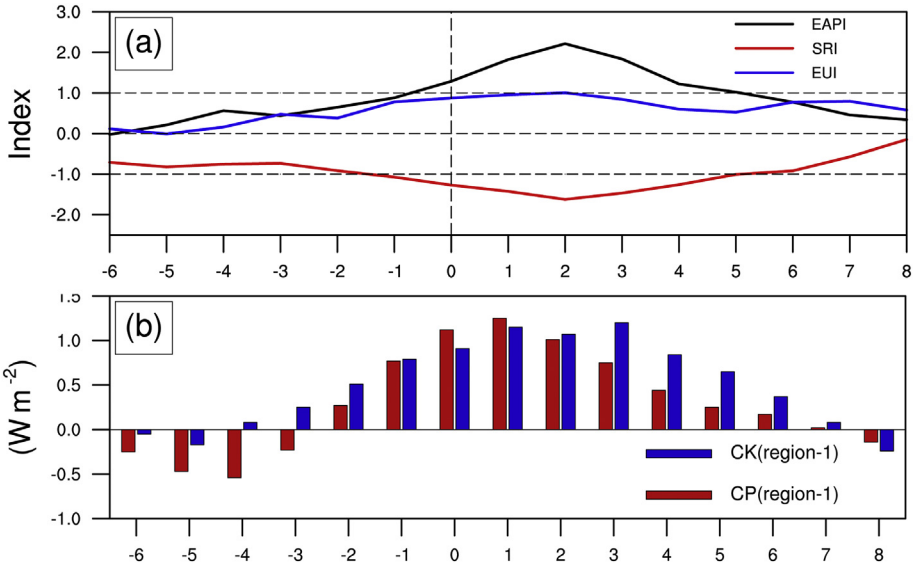

Fig. 7. (a) Composite indices of EAP, SR, and EU patterns from day −6 to day 8. (b) Daily domain-averaged barotropic energy conversion *CK* (W m^{-2}) and baroclinic energy conversion *CP* (W m^{-2}) within the key region marked in Fig. 6 (green rectangles, 105–150°E, 32.5–45°N) from day −6 to day 8. (For interpretation of the references to colour in this figure legend, the reader is referred to the web version of this article.)

Table 2
Time scales (days) of energy conversions (*KE* for τ_{CK}, *APE* for τ_{CP}, and *KE* + *APE* for τ_{CK+CP}) which are horizontally integrated over the region marked in Fig. 6 (105–150°E, 32.5–45°N) during the developing phase of EAP events (day −6 to day −1) and during the peak phase of EAP events (day 0 to day 2). Both the energy and energy conversions have been integrated vertically from the surface to 100 hPa level.

τ (conversion efficiencies)	Day −6 to day −1	Day 0 to day 2
τ_{CK}	40.6 days	23.5 days
τ_{CP}	**1.34 days**	**0.24 days**
τ_{CK+CP}	5.15 days	3.17 days

Time scales shorter than 3 days are shown in bold.

precipitation in the Yangtze River's middle and lower reaches (Müller et al., 2009; Archambault et al., 2010). Accordingly, 105 summer extreme precipitation cases can be identified from the 120 days accumulated by all the selected EAP events, which account for about 26.2% of the total 401 summer extreme precipitation days in the Yangtze River's middle and lower reaches during 1979–2015. Particularly, the synoptic-scale EAP pattern is only one of the favorable factors responsible for summer extreme precipitation in the Yangtze River Valley (Li et al., 2017). For remaining 73.8% summer extreme precipitation cases, it is possible that the EAP-like pattern may also be identified in a particular case, but its intensity is not as conductive as the counterparts in these 19 selected EAP cases (Table 1) and fails to satisfy the criteria of 'a typical EAP case' (Chen and Zhai, 2016). Further, in view of the diversity and complexity of potential mechanisms with respect to summer extreme precipitation in the middle and lower reaches of Yangtze River, for example the influences of typhoons or their remnants, the quasi-stationary Mei-Yu front episodes, and the stagnant upstream blocking episodes (Choi et al., 2010; Chen and Zhai, 2017; Lü et al., 2017), this percentage (26.2%) may highlight the significance of synoptic-scale EAP pattern in inducing summer extreme precipitation.

The synoptic-scale EAP pattern has a profound effect on the occurrence of the summer persistent extreme precipitation (PEP) over the middle and lower reaches of Yangtze River (Lü et al., 2017). Composite analyses further indicate that the tripole structure of synoptic-scale EAP pattern emerges prior to the occurrence of PEP. Thus, it is possible to take daily EAPI as a reliable precursor for summer PEP in the Yangtze River's middle and lower reaches (Wang and Zhang, 2015).

5.2. Precursor and simultaneous large-scale circulation anomalies

Concurrent circulation anomalies are capable of inducing consecutive strong rainfall (Wang et al., 2000; Lau and Weng, 2002; Müller et al., 2009). This section therefore quantifies relationships between the EAP-induced summer PEP and EAP-related circulation anomalies.

From day −6 onward, the SAH and WPSH begin to experience a particularly significant zonal approach (Figs. 3 and 5). By day −2, the west boundary of the WPSH encounters the east boundary of the SAH. During EAP events, an overlap between these two key systems resides over the coastal region of South China for several days, maintaining the precipitation (Jin et al., 2013). As the decay of the EAP pattern, the SAH and WPSH deviate from each other in opposite directions and eventually retreat to their climatological-mean positions, terminating

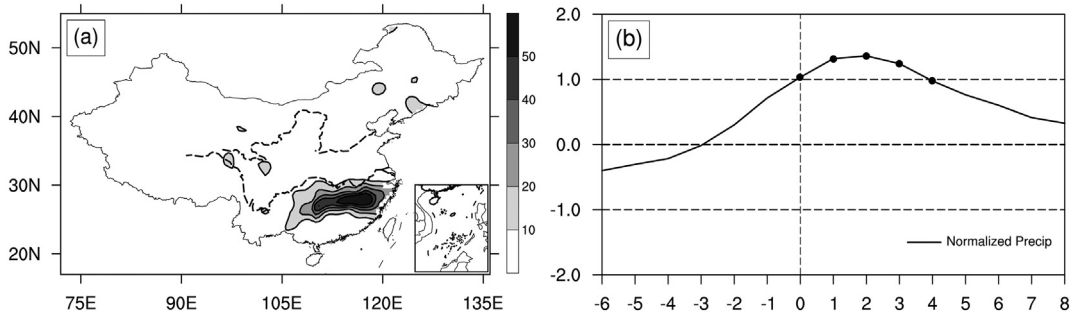

Fig. 8. (a) Spatial distribution of average precipitation (units: mm) during EAP events (from day 0 to day 4) in China. (b) Daily domain-averaged normalized precipitation within the Yangtze River's middle and lower reaches (black rectangles in Fig. 9, 27–32°N, 112.5–120°E) from day −6 to day 8. Statistically significant anomalies (5% level) are highlighted with solid circles.

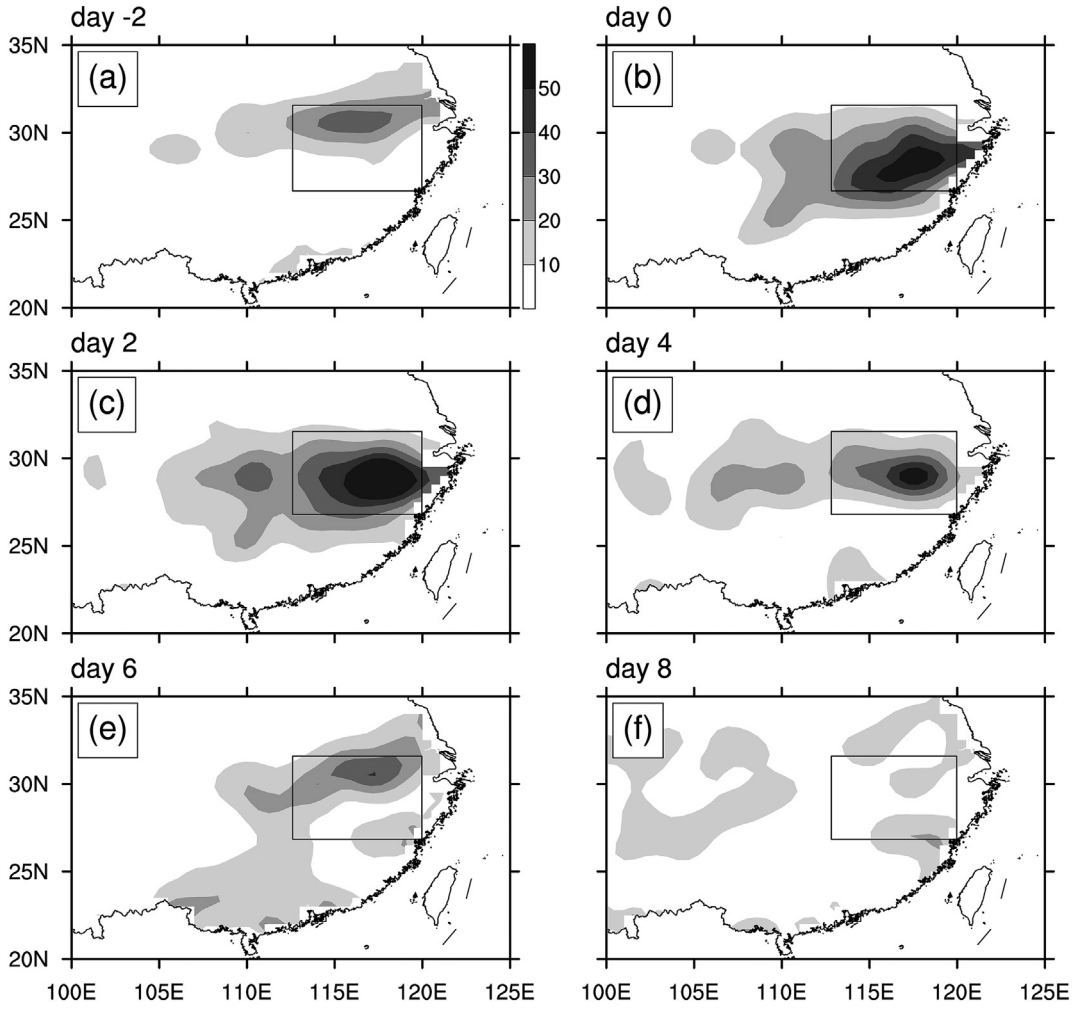

Fig. 9. Precipitation (units: mm) in the Yangtze River's middle and lower reaches (black rectangles, 27–32°N, 112.5–120°E) during the period from day −2 to day 8.

precipitation in the Yangtze River's middle and lower reaches (figure not shown). Previous studies have broadly employed the similar zonal advance between the SAH and WPSH as an effective precursor for East Asian summer rainfall (Lu and Lin, 2009; Jin et al., 2013; Chen and Zhai, 2016).

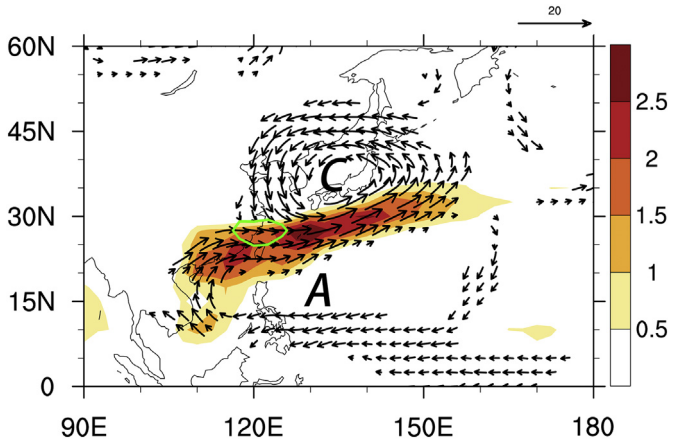

Fig. 10. Distribution of average wind anomalies at 850 hPa (vector; units: $m\ s^{-1}$), normalized anomalies of total moisture flux (shading), and the moisture flux convergence (green contour is $-4 \times 10^{-8}\ s^{-1}$) from day 0 to day 2. (For interpretation of the references to colour in this figure legend, the reader is referred to the web version of this article.)

An anomalous low-level cyclone/anticyclone pair ('C/A' in Fig. 10) centered over the Philippine Sea and the Japan also plays a significant role (Chen and Zhai, 2015; Wang and Wang, 2018). During EAP events, the western boundaries of both low-latitude anticyclonic anomalies and the WPSH can reach 115°E. Because of the further strengthening and westward extension of the WPSH, the reinforced low-level southwesterlies to the northern flank of low-latitude anticyclonic anomalies advect abnormally abundant moisture toward the Yangtze River's middle and lower reaches where the PEP occurred (Xu et al., 2017), leading to a particularly significant moisture flux with a magnitude anomaly over 1.0 standard deviation. The anomalously abundant moisture transport required by precipitation largely deepens on the prevailing southwesterlies related to the intensified WPSH and the anomalous subtropical anticyclone, rather than the southwesterlies originated from the Bay of Bengal (Chen and Zhai, 2017; Gong et al., 2017).

In addition, accompanying development of the mid-latitude cyclonic anomalies is the northerlies from mid-latitudes (45°N), steering the low-level dry/cold air into the Yangtze River's middle and lower reaches. Hence, the confluence between these northerlies and low-latitude southwesterlies greatly enhance the convergence of moisture flux around the Yangtze River's middle and lower reaches (Fig. 10). From day −2, over the convergence areas, a moist and thick layer (represented by specific humidity in Fig. 11) is clearly identified in the lower-middle troposphere. Such leading moisture flux convergence triggers pronounced local ascending motion along a thicker/moister layer at EAP maintenance stage (Fig. 11), providing unstable conditions

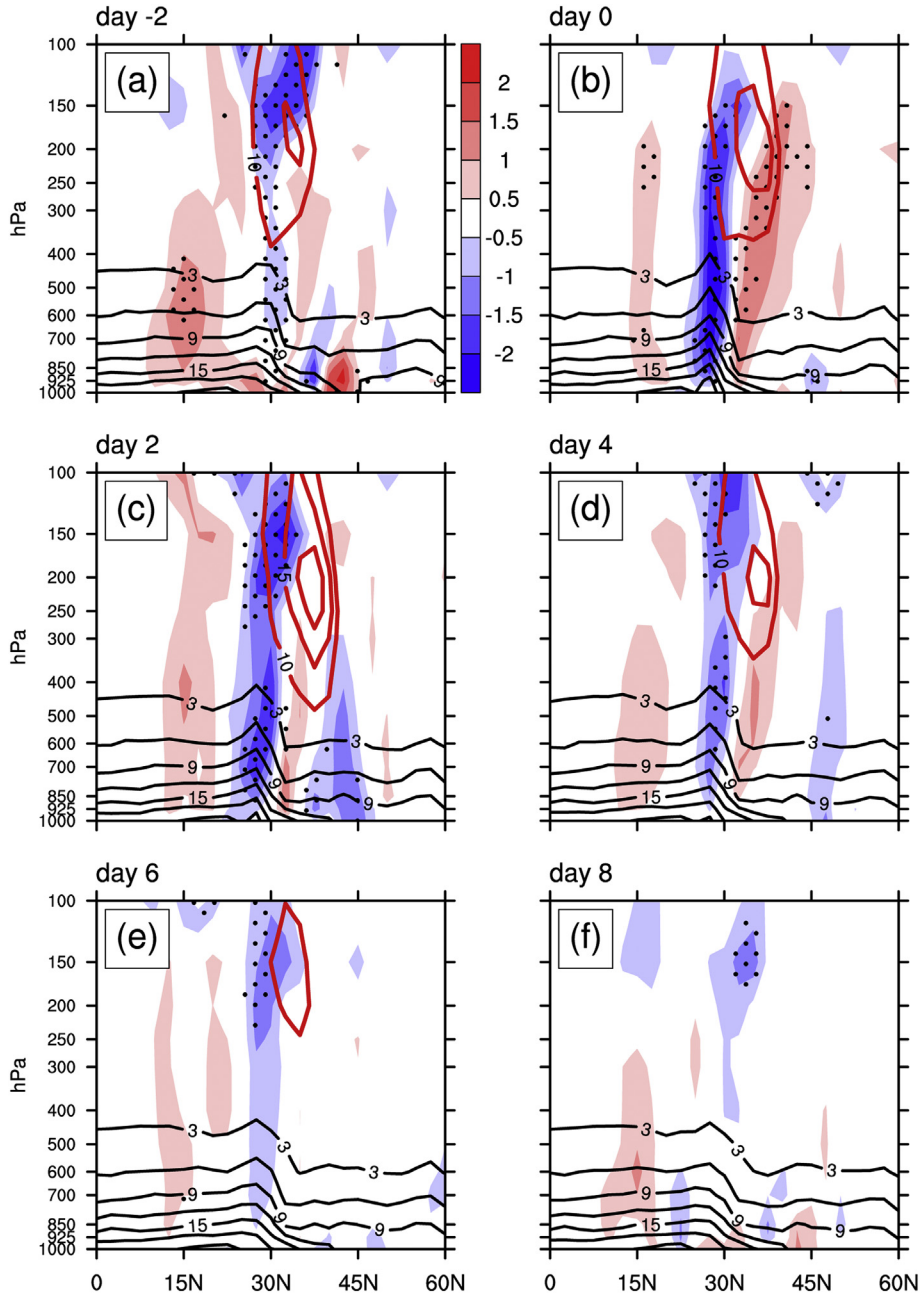

Fig. 11. Latitude-pressure cross-section (112.5–120°E) of specific humidity (black contours; with interval of 3 g kg^{-1}), zonal wind anomalies (red contours; with interval of 5 m s^{-1}), and vertical *p*-velocity anomalies (shading; units: hPa s^{-1}) from day −2 to day 8. Statistically significant vertical *p*-velocity anomalies (5% level) are highlighted by black points. (For interpretation of the references to colour in this figure legend, the reader is referred to the web version of this article.)

for PEP (Wang and Xie, 1996). Moreover, the upper-level strong divergence arising from the accelerating westerly jet (red contours in Fig. 11) favors the development and preservation of local ascents. In nature, such long-lasting strong ascents of moist/warm air along the moist and thick layer largely account for the PEP in the Yangtze River's middle and lower reaches (Jin et al., 2013).

6. Discussion and conclusions

Based on the ECMWF Re-analysis (ERA-Interim) daily datasets and daily gridded precipitation dataset obtained from Chinese Ground Precipitation Gridded Dataset (V2.0), the evolution features and mechanism of East Asia-Pacific (EAP) teleconnection pattern and its potential influence on summer rainfall in China have been examined on synoptic timescales in present study. The main findings of this article can be summarized by a simple schematic diagram (Fig. 12).

EAP pattern can be extracted as the dominant mode during East Asian summer on synoptic timescales, in agreement with previous studies (Chen and Zhai, 2015; Li et al., 2017). Its evolution is inextricably linked to the wave energy propagation represented by the wave-activity flux (WAF) in different levels of the troposphere (Takaya and Nakamura, 2001). In the lower troposphere (Fig. 12a), the poleward energy propagation forced by the convective cooling anomalies around the Philippine Sea, triggers the EAP-related anomalies in sequence from low- to mid-high latitudes and maintains the north-south tripole structure for several days (Huang and Sun, 1994; Nitta and Hu, 1996). In the middle troposphere, the zonally distributed ridge/trough/ridge wave train provides a favorable westerly waveguide for the eastward and southeastward WAFs from the Ural blocking high (Ambrizzi et al., 1995; Takaya and Nakamura, 2001). Accordingly, the

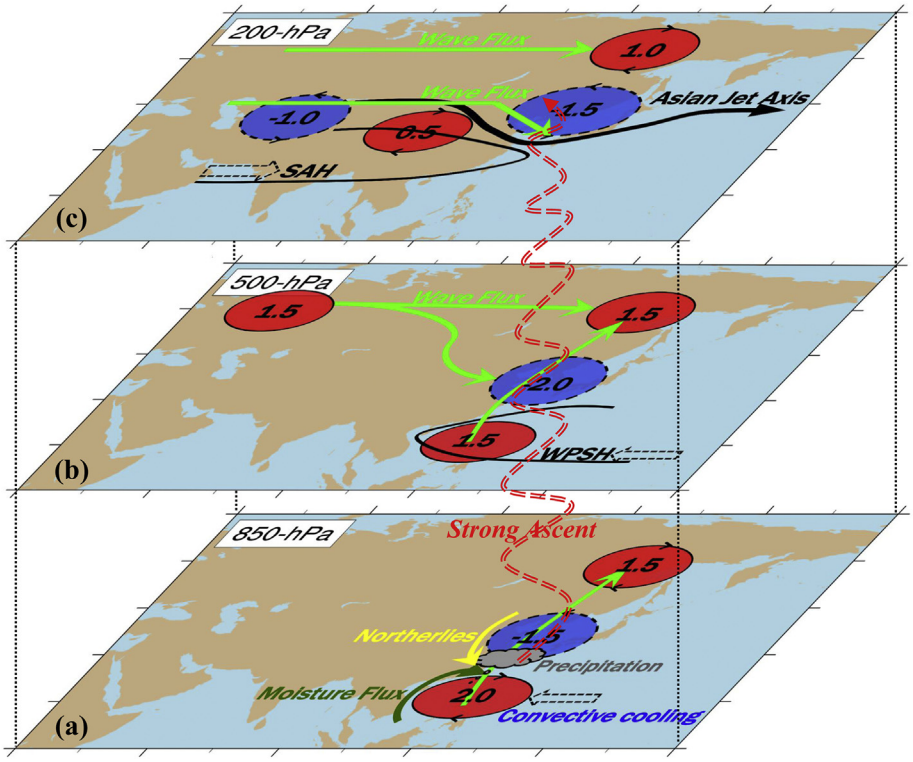

Fig. 12. Schematic diagrams for the wave-activity fluxes required by the evolution of synoptic-scale EAP pattern, and concurrent anomalous circulation patterns responsible for the consecutive strong rainfall in the Yangtze River's middle and lower reaches. The wave fluxes propagations are presented as the bright green arrows. The thick black line in Fig. 12c denotes the Asian jet axis. The yellow arrow in Fig. 12a represents the northerlies. Dark green arrow in Fig. 12a represents the low-level anomalously abundant moisture flux steered by the southwesterlies. The gray 'cloud shape' in Fig. 12a marks the position of precipitation. The strong ascent is presented as a red dashed curve. The blue and red shadings represent the negative and positive height anomaly centers, with the maximum values of normalized anomalies labeled on them. The black solid lines in Fig. 12b and c denote the boundaries of the WPSH and SAH, respectively. The dashed blank arrows represent the shifts of these key systems. (For interpretation of the references to colour in this figure legend, the reader is referred to the web version of this article.)

convergences between the southeastward (eastward) WAFs and poleward WAFs over mid-latitude (high-latitude) East Asia jointly stimulate the advance and preservation of synoptic-scale EAP pattern (Fig. 12b).

Moreover, in the upper troposphere, the anomalies related to the upper-level EAP pattern are primarily affected by two conspicuous eastward WAFs (Fig. 12c). One may contribute to the advance of Okhotsk anticyclonic (positive) anomaly, and the other one associated with the Silk-Road (SR) wave train along the upper-level Asian jet persistently converges into the cyclonic (negative) anomaly to greatly strengthen it (Fujinami and Yasunari, 2009). The rapid dissipation of the high-latitude WAFs leads to a relatively short duration of anticyclonic anomaly; however, the preservation of the SR pattern provides consecutive energy for the long-lasting maintenance of the relatively strong mid-latitude cyclonic anomaly. Furthermore, the energetics diagnoses indicate that the highly efficient baroclinic energy conversion responsible for the self-maintenance of the SR pattern is also capable of reinforcing and maintaining this mid-latitude cyclonic anomaly by extracting the available potential energy from basic flow (Sato and Takahashi, 2006).

In particular, synoptic-scale EAP pattern exerts great impact on summer rainfall of southern China and exhibits a distinct zonal advance and gradual approach between the SAH and WPSH prior to its onset. An overlap between them remains in a favorable position for summer rainfall in the Yangtze River's middle and lower reaches during EAP pattern lifetime (Lu and Lin, 2009; Jin et al., 2013; Wang and Wang, 2018). In nature, the long-lasting strong ascents of moist/warm air along a moist and thick layer within the abnormally abundant moisture convergence areas lead to the summer persistent extreme precipitation (PEP) in the Yangtze River's middle and lower reaches, with precipitation amount of 50 mm day^{-1} or greater for several days.

Present study indicates that EAP-related summer PEP cases in the middle and lower reaches of Yangtze River are featured by the simultaneous existence and concurrent behavior between EAP and SR teleconnection patterns. Based on clarifying the possible interaction between these two key patterns, as they vary earlier than the summer PEP, it is more likely to consider synoptic-scale teleconnections as the precursors for PEP in China. Therefore, more attention should be paid to the formation mechanisms of such combination, the possible interaction between EAP and SR patterns, and the combined effects on the summer precipitation in China.

Acknowledgements

This work was jointly supported by the China Meteorological Administration Special Public Welfare Research Fund Province (GYHY201406024), the Major Program of the Natural Science Researches for Colleges and Universities in Jiangsu Province (14KJA170004), the National Natural Science Foundation of China (41575081), the Research and Innovation Project for College Graduates of Jiangsu Province (No. 1344051501001), the Creative Program of the State Key Laboratory of Severe Weather (2015LASW-A03), and the Priority Academic Program Development of Jiangsu Higher Education Institutions (PAPD).

References

Ambrizzi, T., Hoskins, B.J., Hsu, H.H., 1995. Rossby wave propagation and teleconnection patterns in the austral winter. J. Atmos. Sci. 52, 3661–3672. http://ntur.lib.ntu.edu.tw/bitstream/246246/174968/1/03.pdf.

Archambault, H.M., Keyser, D., Bosart, L.F., 2010. Relationships between large-scale regime transitions and major cool-season precipitation events in the northeastern United States. Mon. Wea. Rev. 138, 3454–3473. https://doi.org/10.1175/2010MWR3362.1.

Chen, Y., Zhai, P.M., 2015. Synoptic-scale precursors of the East Asia/Pacific teleconnection pattern responsible for persistent extreme precipitation in the Yangtze River Valley. Q. J. R. Meteorol. Soc. 141, 1389–1403. https://doi.org/10.1002/qj.2448.

Chen, Y., Zhai, P.M., 2016. Mechanisms for concurrent low-latitude circulation anomalies responsible for persistent extreme precipitation in the Yangtze River Valley. Clim. Dyn. 47, 989–1006. https://doi.org/10.1007/s00382-015-2885-6.

Chen, Y., Zhai, P.M., 2017. Simultaneous modulations of precipitation and temperature extremes in Southern parts of China by the boreal summer intraseasonal oscillation. Clim. Dyn. 49, 3363–3381. https://doi.org/10.1007/s00382-016-3518-4.

Chen, W., Gu, L., Wei, K., Huang, R.H., 2008. Studies of the dynamical processes of East Asian monsoon system and the quasi-stationary planetary wave activities. Chinese J. Atmos. Sci. 32, 950–966 (In Chinese).

Chen, H.S., Teng, F.D., Zhang, W.X., Liao, H., 2017. Impacts of anomalous mid-latitude cyclone activity over East Asia during summer on the decadal mode of East Asian summer monsoon and its possible mechanism. J. Clim. 30, 739–753. https://doi.org/

10.1175/JCLI-D-16-0155.1.
Choi, K.S., Wu, C.C., Cha, E.J., 2010. Change of tropical cyclone activity by Pacific-Japan teleconnection pattern in the western North Pacific. J. Geophys. Res.-Atmos. 115, D19. https://doi.org/10.5322/JESI.2015.24.11.1371.
Dee, D.P., et al., 2011. The ERA-interim reanalysis: configuration and performance of the data assimilation system. Q. J. R. Meteorol. Soc. 137, 553–597. https://doi.org/10.1002/qj.828.
Ding, Y.H., Chan, J.C.L., 2005. The East Asian summer monsoon: an overview. Meteorol. Atmos. Phys. 89, 117–142. https://doi.org/10.1007/s00703-005-0125-z.
Ding, Q.H., Wang, B., 2005. Circumglobal teleconnection in the northern hemisphere summer. J. Clim. 18, 3483–3505. https://doi.org/10.1175/JCLI3473.1.
Ding, Q.H., Wang, B., 2007. Intraseasonal teleconnection between the summer Eurasian wave train and the Indian Monsoon. J. Clim. 20, 3751–3767. https://doi.org/10.1175/JCLI4221.1.
Enomoto, T., Hoskins, B.J., Matsuda, Y., 2003. The formation mechanism of the Bonin high in August. Q. J. R. Meteorol. Soc. 129, 157–178. https://doi.org/10.1256/qj.01.211.
Fujinami, H., Yasunari, T., 2009. The effects of midlatitude waves over and around the Tibetan Plateau on submonthly variability of the East Asian summer monsoon. Mon. Wea. Rev. 137, 2286–2304. https://doi.org/10.1175/2009MWR2826.1.
Gong, Z.Q., Dogar, M.M., Qiao, S.B., Hu, P., Feng, G.L., 2017. Limitations of BCC_CSM's ability to predict summer precipitation over East Asia and the Northwestern Pacific. Atmos. Res. 193, 184–191. https://doi.org/10.1016/j.atmosres.2017.04.016.
Grotjahn, R., Faure, G., 2008. Composite predictor maps of extraordinary weather events in the Sacramento, California, region. Wea. Forecasting 23, 313–335. https://doi.org/10.1175/2007WAF2006055.1.
Grumm, R.H., Hart, R.H., 2001. Standardized anomalies applied to significant cold season weather events: preliminary findings. Wea. Forecasting 16, 736–754. https://doi.org/10.1175/1520-0434(2001)016<0736:SAATSC>2.0.CO;2.
Guan, Z.Y., Yamagata, T., 2003. The unusual summer of 1994 in East Asia: IOD teleconnections. Geophys. Res. Lett. 30, 235–250. https://doi.org/10.1029/2002GL016831.
Hart, R.E., Grumm, R.H., 2001. Using normalized climatological anomalies to rank synoptic-scale events objectively. Mon. Wea. Rev. 129, 2426–2442. https://doi.org/10.1175/1520-0493(2001)129<2426:UNCATR>2.0.CO;2.
Hatzaki, M., Wu, R.G., 2015. The South-Eastern Europe winter precipitation variability in relation to the North Atlantic SST. Atmos. Res. 152, 61–68. https://doi.org/10.1016/j.atmosres.2013.10.008.
Hong, X.W., Lu, R.Y., 2016. The meridional displacement of the summer Asian jet, silk road pattern, and tropical SST anomalies. J. Clim. 29, 3753–3766. https://doi.org/10.1175/JCLI-D-15-0541.1.
Hsu, H.H., Lin, S.M., 2007. Asymmetry of the tripole rainfall pattern during the east Asian summer. J. Clim. 20, 4443–4458. https://doi.org/10.1175/JCLI4246.1.
Hsu, H.H., Weng, C.H., 2001. Northwestward propagation of the intraseasonal oscillation in the western North Pacific during the boreal summer: structure and mechanism. J. Clim. 14, 3834–3850. https://doi.org/10.1175/1520-0442(2001)014<3834:NPOTIO>2.0.CO;2.
Hu, D.Z., Guan, Z.Y., Tian, W.S., Ren, R.C., 2018. Recent strengthening of the stratospheric Arctic vortex response to warming in the central North Pacific. Nat. Commun. 9, 1697. https://doi.org/10.1038/s41467-018-04138-3.
Huang, R.H., 1987. Influence of the heat source anomaly over the tropical western Pacific on the subtropical high over East Asia. In: Proc. International Conference on the General Circulation of East Asia, April 10–15, Chengdu, China, pp. 40–51.
Huang, R.H., Sun, F.Y., 1994. Impact of the convective activities over the western tropical Pacific warm pool on the intraseasonal variability of the east Asian summer monsoon. Chinese J. Atmos. Sci. 146, 289–296 (In Chinese).
Jiang, J., Lu, Y.Y., Perrie, W., 2005. Estimating the energy flux from the wind to ocean inertial motions: the sensitivity to surface wind fields. Geophys. Res. Lett. 32, 291–310. https://doi.org/10.1029/2005GL023289.
Jin, Q., Yang, X.Q., Sun, X.G., Fang, J.B., 2013. East Asian summer monsoon circulation structure controlled by feedback of condensational heating. Clim. Dyn. 41, 1885–1897. http://meetingorganizer.copernicus.org/EGU2013/EGU2013-2814.pdf.
Kawamura, R., Ogasawara, T., 2006. On the role of typhoons in generating PJ teleconnection patterns over the western North Pacific in late summer. SOLA. 2, 37–40. https://doi.org/10.2151/sola.2006-010.
Kawamura, R., Murakami, T., Wang, B., 1996. Tropical and mid-latitude 45-day perturbations over the western Pacific during the northern summer. J. Meteorol. Soc. Japan 74, 867–890. https://ci.nii.ac.jp/els/contentscinii_20180402013223.pdf?id=ART0001949930.
Kosaka, Y., Nakamura, H., 2006. Structure and dynamics of the summertime Pacific–Japan teleconnection pattern. Q. J. R. Meteorol. Soc. 132, 2009–2030. https://doi.org/10.1256/qj.05.204.
Kosaka, Y., Nakamura, H., Watanabe, M., Kimoto, M., 2009. Analysis on the dynamics of a wave-like teleconnection pattern along the summertime Asian jet based on a reanalysis dataset and climate model simulations. J. Meteorol. Soc. Japan 87, 561–580. https://doi.org/10.2151/jmsj.87.561.
Kosaka, Y., Chowdary, J.S., Xie, S.P., Min, Y.M., Lee, J.Y., 2012. Limitations of seasonal predictability for summer climate over East Asia and the northwestern Pacific. J. Clim. 25, 7574–7589. https://doi.org/10.1175/JCLI-D-12-00009.1.
Lau, K.M., Weng, H., 2002. Recurrent teleconnection patterns linking summertime precipitation variability over East Asia and North America. J. Meteorol. Soc. Japan 80, 1309–1324. https://doi.org/10.2151/jmsj.80.1309.
Li, H., Zhai, P.M., Chen, Y., Lu, E., 2017. Potential influence of the East Asia–Pacific teleconnection pattern on persistent precipitation in South China: implications of atypical Yangtze River valley cases. Wea. Forecasting 33, 267–282. https://doi.org/10.1175/WAF-D-17-0011.1.
Liebmann, B., 1996. Description of a complete (interpolated) outgoing longwave radiation dataset. Bull. Amer. Meteorol. Soc. 77, 1275–1277.
Loboda, N.S., Glushkov, A.V., Khokhlov, V.N., 2005. Using meteorological data for reconstruction of annual runoff series over an ungauged area: empirical orthogonal function approach to Moldova–Southwest Ukraine region. Atmos. Res. 77, 100–113. https://doi.org/10.1016/j.atmosres.2004.10.020.
Lu, R.Y., Lin, Z.D., 2009. Role of subtropical precipitation anomalies in maintaining the summertime meridional teleconnection over the western North Pacific and East Asia. J. Clim. 22, 2058–2072. https://doi.org/10.1175/2008JCLI2444.1.
Lu, R.Y., Oh, J.H., Kim, B.J., 2002. A teleconnection pattern in upper-level meridional wind over the North African and Eurasian continent in summer. Tellus 54, 44–55. https://doi.org/10.3402/tellusa.v54i1.12122.
Lü, J.M., Li, Y., Zhai, P.M., Chen, J.M., 2017. Teleconnection patterns impacting on the summer consecutive extreme rainfall in Central–Eastern China. Int. J. Climatol. 37, 3367–3380. https://doi.org/10.1002/joc.4923.
Müller, M., Kašpar, M., Řezáčová, D., Sokol, Z., 2009. Extremeness of meteorological variables as an indicator of extreme precipitation events. Atmos. Res. 92, 308–317. https://doi.org/10.1016/j.atmosres.2009.01.010.
Nakamura, H., Fukamachi, T., 2004. Evolution and dynamics of summertime blocking over the Far East and the associated surface Okhotsk high. Q. J. R. Meteorol. Soc. 130, 1213–1233. https://doi.org/10.1256/qj.03.101.
National Meteorological Information Center, 2010. Assessment Report of China's Ground Precipitation 0.5° × 0.5° Gridded Dataset (V2.0). National Meteorological Information Center, Assessment Report of China's Ground, Beijing, China.
Nitta, T., 1987. Convective activities in the tropical western Pacific and their impact on the Northern Hemisphere summer circulation. J. Meteorol. Soc. Japan 65, 373–390. https://doi.org/10.2151/jmsj1965.65.3_373.
Nitta, T., Hu, Z.Z., 1996. Summer climate variability in China and its association with 500 hPa height and tropical convection. J. Meteorol. Soc. Japan 74, 425–445. https://doi.org/10.2151/jmsj1965.74.4_425.
North, G.R., Bell, T.L., Cahalan, R.F., Moeng, F.J., 1982. Sampling errors in the estimation of empirical orthogonal functions. Mon. Wea. Rev. 110, 699–706. https://doi.org/10.1175/1520-0493(1982)110<0699:SEITEO>2.0.CO;2.
Sato, N., Takahashi, M., 2006. Dynamical processes related to the appearance of quasi-stationary waves on the subtropical jet in the midsummer Northern Hemisphere. J. Clim. 19, 1531–1544. https://doi.org/10.1175/JCLI3697.1.
Shi, N., Bueh, C., Ji, L.R., Wang, P.X., 2009. The impact of mid-and high-latitude Rossby wave activities on the medium-range evolution of the EAP pattern during the pre-rainy period of South China. J. Meteorol. Res. 23, 300–314.
Simmons, A.J., Wallace, J.M., Branstator, G.W., 1983. Barotropic wave propagation and instability, and atmospheric teleconnection patterns. J. Atmos. Sci. 40, 1363–1392. https://doi.org/10.1175/1520-0469(1983)040<1363:BWPAIA>2.0.CO;2.
Takaya, K., Nakamura, H., 1997. A formulation of a wave-activity flux for stationary Rossby waves on a zonally varying basic flow. Geophys. Res. Lett. 24, 2985–2988. https://doi.org/10.1029/97GL03094.
Takaya, K., Nakamura, H., 2001. A formulation of a phase-independent wave-activity flux for stationary and migratory quasigeostrophic eddies on a zonally varying basic flow. J. Atmos. Sci. 58, 608–627. https://doi.org/10.1175/1520-0469(2001)058<0608:AFOAPI>2.0.CO;2.
Wakabayashi, S., Kawamura, R., 2004. Extraction of major teleconnection patterns possibly associated with the anomalous summer climate in Japan. J. Meteorol. Soc. Japan 82, 1577–1588. https://doi.org/10.2151/jmsj.82.1577.
Wang, C., Wang, L.J., 2018. Combined effects of synoptic-scale teleconnection patterns on summer precipitation in southern China. Atmos. 9, 154. https://doi.org/10.3390/atmos9040154.
Wang, B., Xie, X.S., 1996. Low-frequency equatorial waves in vertically sheared zonal flow. Part I: stable waves. J. Atmos. Sci. 53, 449–467. https://doi.org/10.1175/1520-0469(1996)053<0449:LFEWIV>2.0.CO;2.
Wang, N., Zhang, Y.C., 2015. Evolution of Eurasian teleconnection pattern and its relationship to climate anomalies in China. Clim. Dyn. 44, 1017–1028. https://doi.org/10.1007/s00382-014-2171-z.
Wang, B., Wu, R.G., Fu, X.H., 2000. Pacific–east Asian teleconnection: how does ENSO affect east Asian climate? J. Clim. 13, 1517–1536. https://doi.org/10.1175/1520-0442(2000)013<1517:PEATHD>2.0.CO;2.
Xu, W.X., Jiang, H.Y., Kang, X.B., 2014. Rainfall asymmetries of tropical cyclones prior to, during, and after making landfall in South China and Southeast United States. Atmos. Res. 139, 18–26. https://doi.org/10.1016/j.atmosres.2013.12.015.
Xu, M., Kang, S.C., Wu, H., Yuan, X., 2017. Detection of spatio-temporal variability of air temperature and precipitation based on long-term meteorological station observations over Tianshan Mountains, Central Asia. Atmos. Res. 203, 141–163. https://doi.org/10.1016/j.atmosres.2017.12.007.
Yanai, M., Esbensen, S., Chu, J.H., 1973. Determination of bulk properties of tropical cloud clusters from large-scale heat and moisture budgets. J. Atmos. Sci. 30, 611–627. https://doi.org/10.1175/1520-0469(1973)030<0611:DOBPOT>2.0.CO;2.